Image Signal Modulation and Noise Analysis of CRT Displays

Peter D. Burns

Imaging Information Systems - Research Laboratories
Eastman Kodak Company, Rochester, New York 14653-5712

ABSTRACT

The image modulation and noise characteristics of monochrome cathode ray tube (CRT) displays are described using a simple physical model. The model includes digital-to-analog converter, the video amplifier, electron gun, phosphor and faceplate. Expressions are derived for both the signal modulation transfer function (MTF) and noise power spectrum in the terms of the subsystem characteristics.

1. INTRODUCTION

Cathode ray tube (CRT) displays are now the most frequent way in which information is extracted from many electronic imaging systems. Applications for CRT displays include not only many for direct viewing, but also those for photographic film exposure[1] for pictorial and data recording.[2] In all these systems, various technologies are combined in order to acquire, process and display image information. Understanding the characteristics of the display is important, since it can limit system image quality. Evaluation of CRT displays is often done in terms of physical imaging characteristics,[3-5] which can be used to evaluate visual measures such as sharpness.[6-9]

Our intent here is to develop a simple physical model that could be used to provide insight into measured or observed performance, or to specify CRT imaging characteristics. Evaluation of various designs and competing technologies is facilitated by a consistent description of signal modulation and noise characteristics[10,11]. In addition, signal-to-noise ratio techniques can be used to evaluate ultimate performance,[12] or that limited by other functions such as image acquisition.[13] This approach requires a description of imaging performance of each element in the imaging chain. System design can then be optimized for a given application based on specific imaging requirements, such as information capacity, fidelity[14-16] or explicit visual criteria.[17,18]

We start with a model of the imaging steps from digital signal to output image for a monochrome CRT display. The model includes digital-to-analog converter, video amplifier, electron gun, and phosphor characteristics. Expressions are derived for both the signal modulation transfer function (MTF) and noise power spectrum in the terms of the subsystem characteristics.

In order to describe the physical characteristics of each step in the CRT signal path, several image parameters will be addressed at each stage. Expressions for the signal MTF will be developed, based on the subsystem signal modulation characteristics. In addition, the Wiener, or noise power spectrum is expressed in terms of the various noise sources. The effects of the various imaging steps on signal and noise will vary in extent and orientation in the image. Here we express the imaging characteristics (i.e., transfer functions and noise sources) in terms of the output image dimensions. The display will be oriented so x is parallel to the fast scan direction of the raster. Most sources that are both independent of, and functions of the mean signal level will be addressed. Artifacts due to aliasing errors, registration errors, or time varying phenomena, such as flicker, will not be addressed. We also limit the analysis by assuming symmetrical spread functions. For imaging systems exhibiting asymmetric spread functions, each component MTF would be substituted with the corresponding optical transfer function. The imaging of specific signals can then be quantified.

For our purposes we will consider the CRT and associated electronics, as shown in the diagram of Fig. 1. The input digital signal is converted to a continuous function by a digital-to-analog converter. This signal is then amplified by the video amplifier that drives the electron gun. This assembly generates the electron beam current as a function of the amplified image signal. The focused beam is swept in raster format across the phosphor, which

coats the inside of the glass faceplate. Electrons are absorbed by the phosphor that generates visible light as an image transmitted by the faceplate to the viewer.

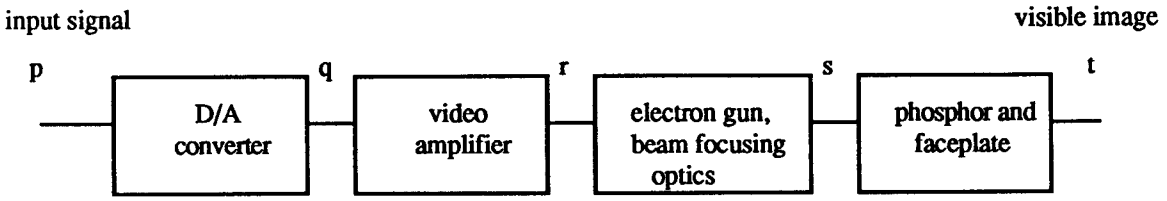

Figure 1. Functional diagram for the CRT model.

2. MODEL

The first step in the CRT signal path is the conversion of the digital image signal into a continuous time function by the analog-to-digital converter. When compared to an original input image, the signal after quantization and digital-to-analog conversion will contain errors due to the finite number of levels used for intermediate storage and processing. The number of quantization levels used for image storage is based on the system input image and output image quality requirements. For example, document processing systems will often quantize, after image processing, to one bit, or two levels. Continuous tone systems, such as for medical imaging applications, often process and quantize images in ten bits. Since aliasing noise due to sampling or interpolation is not being addressed here, we consider the process of digitizing and reconstructing a continuous image as modeled by the addition of a quantization noise. If we make the usual assumption of a uniform distribution for the quantization error,[19] the variance is given by

$$\sigma_b^2(\mu_q) = \frac{\Delta q^2(\mu_q)}{12}$$

where Δq is the quantization interval expressed as a function of the average input signal, μ_q. For uniform quantization this expression becomes

$$\sigma_b^2 = \frac{q_{max}^2}{2^{2b}\,12} \tag{1}$$

where q_{max} is the maximum signal and b is the number of bits used to encode the signal. This treatment of quantization is appropriate for cases where image information is distributed over many quantization levels and the errors are uncorrelated with the signal. The D/A converter can also reduce the signal modulation, due to its finite bandwidth, and introduce stochastic noise. For simplicity, however, these effects will be lumped with the corresponding characteristics of the next stage, the video amplifier.

The video amplifier transforms the output of the D/A converter to a voltage signal used to drive the electron gun. The amplifier can be characterized by a frequency response and stochastic noise source. Often the frequency response of the video amplifier results in greater gain applied to higher frequencies compared to lower frequencies (highpass). This is aimed at increasing the sharpness of the displayed image, but often results in 'ringing' near edges or lines. The video amplifier output impedance can vary with signal level, due to the cathode capacitance that causes the frequency response to vary. We adopt a simplification by assuming that the effective response varies only with the average signal drive level. The amplifier frequency response is often modeled as a 2-pole linear filter.[20]

The signal at the output of the video amplifier can be expressed

$$r(x,y) = \{q(x,y) + \tilde{n}_b(x,y)\} * h_a(x, \mu_r) + \tilde{n}_a(x,y) \tag{2}$$

where * indicates convolution, h_a is the video amplifier impulse response,[21] and $\tilde{n}_a$ is the amplifier noise source. The corresponding noise power spectrum, for a uniform input signal is

$$S_r(u,v) = S_b H_a^2(u) + S_a(u,v), \tag{3}$$

where H_a is the amplifier MTF, S_b and S_a are the noise power spectra of the quantization and video amplifier noise sources. The arguements u and v are the spatial frequency variables corresponding to the x and y dimensions, respectively. In equations (2) and (3), the video amplifier is shown as influencing signal and noise characteristics only in the fast scan, x (and u), dimension.

The output of the video amplifier then modulates the current of the beam generated by the electron gun. The mean signal characteristic, which relates the input drive voltage to the beam current, is usually of the form[22]

$$\mu_s = G(\mu_r) = K \mu_r^{\gamma} \tag{4}$$

where μ_s and μ_r are the mean input and output signals, respectively, and γ has typical values of 1.5 - 2.5. The values of the two constants of equation (4) are the result of the specific anode design and the cutoff voltage.

The modulated beam intensity is assumed to follow a Gaussian cross-section but it is usually not symmetrical. In general, the electron beam width increases with increased signal level. Often CRT designs incorporate a correction circuit or beam truncation aperture to limit this characteristic.[23] To describe the effect of the electron gun on the signal modulation, we first express the modulated anode current in terms of the input, as in equation (4). This is then spatially convolved with the beam profile.[20] This can be expressed as

$$s(x', y') = \int_{-\infty}^{\infty}\int_{-\infty}^{\infty} G[r(x,y)]\, h_g(x-x', y-y')\, dx\, dy$$

where h_g is the beam profile expressed as a shift-invariant function. The (small signal) MTF from input to beam intensity is, therefore

$$T_s(u,v,\mu_s) = H_a(u,v)\, H_g(u,v,\mu_s) \tag{5}$$

Here we have expressed the spatial convolution integral as a multiplication in the frequency domain.

Since the transformation from drive voltage to beam current is assumed to be noise-free. If we assume that the noise fluctuations in r are small compared to the mean signal then

$$S_s(u,v) = \left(K \gamma \mu_r^{\gamma-1}\right)^2 H_g^2(u,v,\mu_s)\, S_r(u,v)\ , \tag{6}$$

where $dG/d\mu_r = K \gamma \mu_r^{\gamma-1}$.

An additional source of reduced image modulation is the deflection system. When the beam profile at the CRT anode (phosphor) is measured, it is usually found to vary as a function of location. This can be compensated for by modified magnetic or electric fields in synchronization with the scanning of the deflected beam.[23] For our purposes

any distortion introduced by the deflection system will be lumped in the effective electron beam profile, $h_g(x,y)$. The deflection and beam forming optics of the CRT cause the modulated beam to form a spot (the beam profile) on the phosphor. A single pixel spot is the image of the source near the cathode that is produced by the main lens. Considerable effort is often expended to reduce the spot size in order to increase the visible image resolution. Successful designs need to trade off a reduction in lens magnification and screen brightness, and increased spherical aberration.

The bombardment of the phosphor and the generation of the visible image, cathodoluminescence, can functionally be described in terms of electron absorption, photon generation and scattering. This shown in Fig. 2. Electrons entering the phosphor are first scattered, then a fraction are absorbed. Several mechanisms account for the electron losses before absorption.[24] Energy absorbed from the electrons is emitted as visible light with an efficiency, η, generally less than one. The visible light is then scattered in the phosphor before exiting through the glass faceplate to be viewed or recorded.

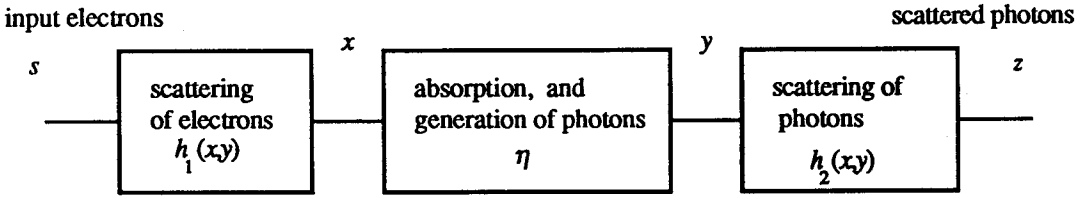

Figure 2. Simple stochastic scattering and absorption model.

The scattering of electrons prior to absorption will be considered to be a stochastic scattering process. The spread function of this process, $h_1(x,y)$, is the probability density function associated with the location of the electron after scattering. The signal MTF associated with this scattering is merely the Fourier transform of $h_1(x,y)$. By applying the approach of Rabbani *et al*,[25] the noise power spectrum of the scattered electron image is given by

$$S_x = (S_s - \mu_s) H_1^2 + \mu_s \tag{7}$$

The first term represents the multiplication of the square of the MTF with the correlated component of the input process that is characterized by $(S_r - \mu_r)$. The second term, μ_r represents the uncorrelated, Poisson distributed, component of $\{r\}$. This expression is consistent with the fact that the spectral density of a completely uncorrelated exposure process is unchanged by scattering.

There are several causes that reduce phosphor efficiency,[24] however, we lump them as an effective parameter, η, which will be a function of wavelength and other factors. The parameter η is the mean number of photons/input electron, or the chance of an incident electron generating a photon. We will assume that this stochastic loss mechanism operates as a nonscattering lossy filter which is a special case of stochastic amplification discussed in Ref. 25. The noise power spectrum of the generated photons is

$$S_y = \eta^2 S_x + \sigma_\eta^2 \mu_x \ .$$

For a binomial selection process, where

$$\sigma_\eta^2 = \eta\,(1-\eta)$$

this becomes

$$S_y = \eta^2 S_x + (\eta - \eta^2)\,\mu_x \ . \tag{8}$$

The photon scattering in the phosphor can also be considered to be a stochastic process, thus the noise power spectrum is given by

$$S_z = (S_y - \mu_y)\, H_2^2 + \mu_y \tag{9}$$

Combining equations (7), (8) and (9) and noting that

$$\mu_z = \mu_y = \eta\, \mu_x = \eta\, \mu_s$$

results in

$$S_z = \eta^2 (S_s - \mu_s)\, H_1^2\, H_2^2 + \mu_s \tag{10}$$

This equation can be simplified if we define an effective phosphor MTF,

$$H_p(u,v) = H_1(u,v)\, H_2(u,v)\ , \tag{11}$$

$$S_z = \eta^2 (S_s - \mu_s)\, H_p^2 + \mu_s \tag{12}$$

In the above approach to describing the signal modulation characteristics we have not identified any of the physical variables, such as phosphor grain morphology, that contribute to the stochastic amplification and scattering. The above analysis, however, can be used to estimate lower limits to image noise. In general, spatial variations in absorption will tend to introduce additional fluctuations at lower spatial frequencies. The net effect of nonuniformities (i.e., distributions of physical parameter values) and those components of equation (12) will be the addition of a noise source whose spectral density falls with spatial frequency. This is consistent with the frequently observed 1/frequency spectrum shape.

The final imaging step is the propagation of the visible light from the phosphor/glass interface to the user. Since scattering precedes the light propagation in the glass faceplate, light approaches the interface as a somewhat diffuse source. Consequently, the visible light can undergo refraction at the interface and internal reflection in the faceplate. The resulting halation[26] has been analyzed in terms of a physical model[27] that explicitly includes phosphor reflection, glass thickness, glass/air reflection, and other properties.

The faceplate halation is seen as a background haze in the image. This can be modeled by the introduction of an additional stochastic scattering mechanism into the signal path. It should be noted that, due to the large extent of the effective spread function, $h_f(x,y)$, this mechanism is often effectively modeled or simulated by the addition of a constant exposure to the image. As in equation (11) and (12), the visible output image is characterized by a system MTF,

$$MTF(u,v) = H_a(u,v)\, H_g(u)\, H_p(u,v)\, H_f(u,v)\ , \tag{13}$$

and output noise power spectrum

$$S_t = \eta^2 (S_s - \mu_s)\, H_p^2\, H_f^2 + \mu_s\ . \tag{14}$$

Substituting equations (3), (6) and (12) into (14),

$$S_t(u,v) = \eta^2 \left[\left(K\ \gamma\, \mu_r^{\gamma-1}\right)^2 (S_b(u,v)\, H_a^2(u,v) + S_a(u,v)) - \mu_s \right] H_g^2(u,v)\, H_p^2(u,v)\, H_f^2(u,v) + \mu_s\ . \tag{15}$$

The various components of the CRT imaging model are shown in the diagram of Fig. 3. Each component characteristic transfer function and noise source of equations (13) - (15) is identified.

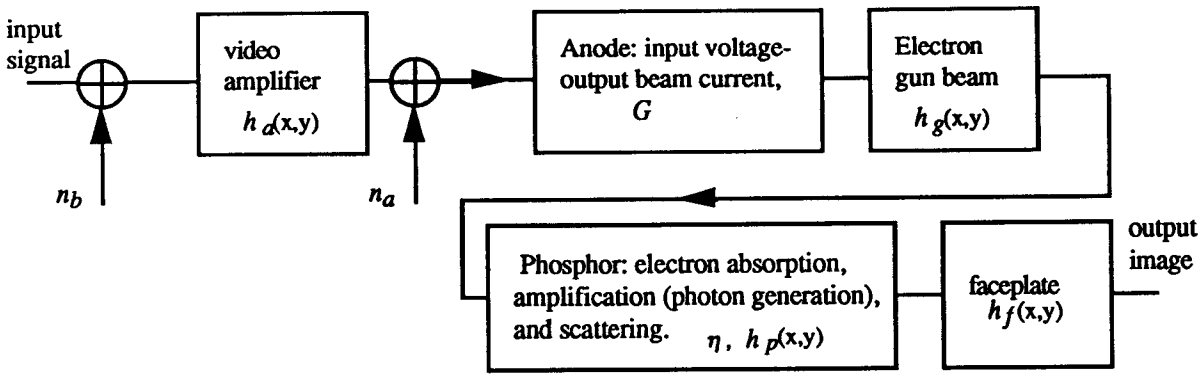

Figure 3. Diagram of CRT imaging model.

4. CONCLUSIONS

Analysis of the signal modulation and noise characteristics of CRT displays has been given in terms of a physical imaging model. Use of such a model allows the interpretation of design choices in terms of overall system requirements, and of observed performance. Since the approach is consistent with established techniques for image signal and noise characterization it can facilitate the comparison between, and optimization of various electro-optical systems.

5. REFERENCES

1. For example, L. Beiser, "A Unified Approach to Photographic Recording from the Cathode-Ray Tube," *Photogr. Sci. Eng.*, 7: 196-204, (1963).
2. M. E. Dunham, and P. E. Sanchez, "Ultimate Sensitivity and Resolution of Phosphor/Fiber/Charge-Coupled Device Systems," *Opt. Eng.*, 26: 1035-1042 (1987).
3. H. L. Snyder, M. Almagor and D. I. Shedivy, "Raster-Scan Display Photometric Noise Measurement," *Aerospace Med. Res. Lab. Report* AMRL-TR-79-13, June 1979.
4. P. G. J. Barten, "Resolution of Data Display Tubes," *Proc. SID*, 25: 35-42 (1984).
5. H. Roehrig et al, "Physical Evaluation of CRT's for use in Digital Radiography," *Proc. SPIE*, 1091: 262-278 (1989).
6. E. M. Granger and K. N. Cupery, "An Optical Merit Function (SQF), Which Correlates with Subjective Image Judgements," *Photogr. Sci. Eng.*, 16: 221-230 (1972).
7. R. Kronlage, "Two-Dimensional Figure of Merit for the Eye and for CRT Raster Displays," *Proc. SPIE*, 29: 119-130 (1988).
8. P. G. J. Barten, "Evaluation of CRT Displays with the SQRI Method," *Proc SID*, 30: 9-14 (1989).
9. H. Isono, "A Real-Time Measurement System to Evaluate Image Sharpness for CRT Displays," *Systems and Computers in Japan*, 19: 58-67 (1988).
10. O. H. Schade, Image Quality a Comparison of Photographic and Television Systems, RCA Labs, Princeton, N J, 1975.
11. R. Shaw, "Comparative Signal-to-Noise Ratio Analysis of Particle Development in Electrophotography and Silver Halide Photography," *J. Appl. Photogr. Eng.* 1: 1-4 (1975).
12. J. C. Dainty and R. Shaw, Image Science, Academic Press, London, 1974, ch.8.

13. P. D. Burns, "Signal-to-Noise Ratio Analysis of Charge-Coupled Device Imagers," *Proc. SPIE*, 1242: 187-194 (1990).
14. F. O. Huck and C. L. Fales, N. Halyo, R. Samms and K. Stacy, "Image Gathering and Processing: Information and Fidelity," *JOSA/A*, 2: 1644-1665 (1985).
15. W. T. Cathey, B. R. Freiden, W. T. Rhodes and C. K. Rushforth, "Image Gathering and Processing for Enhanced Resolution," *JOSA/A*, 1: 241-250 (1984).
16. R. Shaw, "Quality Criteria for Quantized Images," *Proc. SPIE*, 901: 139-143 (1988).
17. S. Ohtsuka, M. Inoue and K. Watenabe, "Quality Evaluation of Pictures with Multiple Impairments Based on Visually Weighted Errors," *Proc. SID*, 30: 3-8 (1989).
18. S. Daly, "Application of a Noise-Adaptive Contrast Sensitivity Function to Image Data Compression," *Opt. Eng.*, 29: 977-987 (1990).
19. A. V. Oppenheim and R. W. Schafer, Digital Signal Processing, Prentice Hall, Engelwood Cliffs, N. J., 1975, pp. 409-413.
20. J. G. Hagerman, "Video Risetime Requirements for Computer-Driven Raster-Scan CRT Displays," *SID 90 Digest*, pp.148-151 (1990)
21. C. Infante, "On the Resolution of Raster-Scanned CRT Displays," *Proc. SID*, 26: 23-36 (1985).
22. H. Moss, Narrow Angle Electronic Guns and Cathode Ray Tubes, Academic Press, NY, 1968, ch.2.
23. T. Okada, "Electronic Displays Conform to CAD/CAM EWS Use," *Display Device '90*, No. 2: 13-17 (1990).
24. S. Larach and A. E. Hardy, "Some Aspects of Cathodoluminescent Phosphors and Screens," *Proc. SID*, 16: 21-30, (1975).
25. M. Rabbani, R. Shaw and R. VanMetter, "Detective Quantum Efficiency of Imaging Systems with Amplifying and Scattering Mechanisms," *JOSA/A* 4: 895-901 (1987).
26 J. D. Rancourt, "Anti-Halo Coatings for Cathode Ray Tube Faceplates," *Proc. SID*, 25: 43-47 (1984).
27. E. B. Gindele and S. L. Shaffer, "A Physical Optics CRT Faceplate Halation Model," *SID 90 Digest* pp. 446-450 (1990).